# UC Riverside
## 2018 Publications

### Title
Fundamentals of Micrometeorology and Dispersion

### Permalink
https://escholarship.org/uc/item/8783r79p

### Authors
Venkatram, A.
Schulte, N.

### Publication Date
2018

Peer reviewed

eScholarship.org Powered by the California Digital Library
University of California

CHAPTER THREE

# Fundamentals of Micrometeorology and Dispersion

## Contents



## INTRODUCTION

This chapter provides the background in the physics of the atmospheric boundary layer that is required to understand transport and dispersion of pollutants associated with the transportation sector. This is followed by an examination of the processes that govern transport and dispersion. We then introduce the models that are used to represent the

*Urban Transportation and Air Pollution.*
DOI: https://doi.org/10.1016/B978-0-12-811506-0.00003-8
© 2018 Elsevier Inc.
All rights reserved.

processes. In Chapter 4, The Impact of Highways on Urban Air Quality, we go into the details of these models.

## SURFACE ENERGY BALANCE—ATMOSPHERIC BOUNDARY LAYER

The atmospheric boundary layer refers to the layer next to the ground that is governed by heat and mass transfer from the earth's surface to the overlying atmosphere. The dynamics of the atmospheric boundary layer is governed by the input of energy from the ground into the boundary layer. The ultimate source of this energy is the sun that supplies the solar radiation to the ground. Solar radiation from the sun provides the energy to generate both the winds and the turbulence in the atmospheric boundary layer. The mean radiant flux outside the earth's atmosphere normal to the solar beam is about 1350 $W/m^2$, most of which lies at wavelengths below 4 μm. Ozone and oxygen in the upper atmosphere absorb most of the energy below 0.3 μm, which accounts for about 3% of the total solar energy. A further 17% is absorbed by water vapor and scattered by particles in the atmosphere, so that about 80% of the radiation incident on the earth's atmosphere reaches the earth's surface. This situation is altered considerably in the presence of clouds, which can scatter most of the energy in the direct beam of solar radiation. Part of this scattered energy goes back into space, while the rest is directed toward the earth. The scattered radiation is referred to as the diffuse component of the solar radiation.

Part of the solar radiation reaching the ground is reflected, and part of it is absorbed. The absorbed solar radiation is converted into other forms through an energy balance at the ground. The components of the energy balance are shown in Fig. 3.1.

Notice that the radiative input to the surface has been separated into solar and thermal radiation. Solar radiation refers to the wavelength region corresponding to the radiation from the sun, whose effective blackbody temperature is close to 6000 K. Most of the solar energy lies in the wavelength region $0 \leq \lambda \leq 4$ μm, with the peak of spectrum at around 0.5 μm.

Thermal radiation refers to energy emitted at temperatures typical of the earth's surface, about 300 K. The energy lies in the region

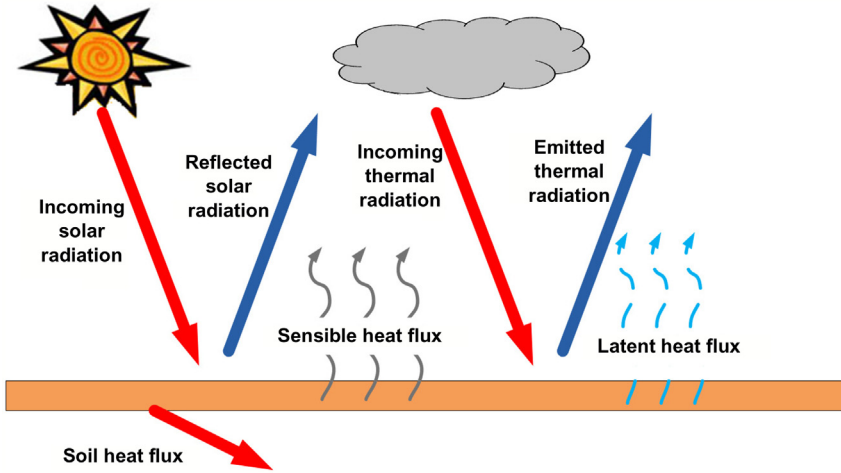


**Figure 3.1** The surface energy balance.

$4 \leq \lambda \leq 100\ \mu m$, with the peak of the spectrum at about $10\ \mu m$. The incoming thermal radiation refers to that emitted by the component gases of the atmosphere, such as water vapor and carbon dioxide, and other so-called greenhouse gases. The outgoing thermal radiation is the energy emitted by the ground. Because the ground is usually warmer than the atmosphere, the outgoing thermal radiation usually exceeds the incoming thermal radiation.

The sensible heat flux is the energy flux from the atmosphere to the ground because of temperature differences between the ground and the atmosphere. During the daytime, energy flows away from the ground into the atmospheric boundary layer, while during the night the boundary layer supplies energy to the ground.

The latent heat flux refers to the energy used to evaporate moisture from the ground. The soil heat flux refers to the energy that is supplied to the ground, and which ultimately determines the temperature of the soil layer.

We are now in a position to write the energy flux balance at the interface between the atmospheric boundary layer and the soil. The surface energy balance reads:

$$R_N = H + L + G, \tag{3.1}$$

where $R_N$ is the net radiation, which is the difference between the solar radiation absorbed at the surface and the net thermal radiation emitted by

the surface. $H$ is the sensible heat flux supplied to the boundary layer, $L$ is the latent heat flux related to the evaporation of water from the surface, and $G$ is the heat flux into the soil.

During the day, $H$ is usually greater than zero, i.e., heat is supplied to the atmosphere. During the night, $H$ is less than zero, i.e., heat is drawn from the atmosphere and the ground to support the cooling of the ground as $R_N$ becomes negative. The cooling can be inhibited in the presence of clouds which radiate energy toward the ground.

When the ground is moist, most of the incoming radiation can go toward evaporation. An approximate method of accounting for energy going into evaporation is to assume that the ratio of latent heat flux to sensible heat flux is a number, referred to as the Bowen ratio, that depends only on the type of surface being considered. Some commonly used methods to calculate the components of the surface energy balance are described in Van Ulden and Holtslag (1985).

## TURBULENCE IN THE ATMOSPHERIC BOUNDARY LAYER

Turbulence is the term applied to atmospheric motion that is so complex that it does not allow for a deterministic description from a practical point of view; we have to be satisfied with understanding the statistical properties of the flow. Turbulent flows occur when the inertial forces acting on the fluid are much greater than the stabilizing viscous forces. The Reynolds number is a measure of the ratio of these two forces. It is defined by

$$\mathrm{Re} = \frac{ud}{\nu}, \tag{3.2}$$

where $u$ is the mean velocity of the flow, $d$ is the length scale of the flow (e.g., the diameter of the pipe through which the fluid is flowing), and $\nu$ is the kinematic viscosity of the fluid. For air, $\nu = 15 \times 10^{-6}\ \mathrm{m^2/s}$. Turbulent flows are characterized by Reynolds numbers much greater than 1000. Fig. 3.2 shows the time variation of the horizontal velocity measured in turbulent flow.

It is common practice to study turbulence using either time averages or something called ensemble averages, which we will not discuss here. If we assume that the flow is steady in the sense that time averages converge

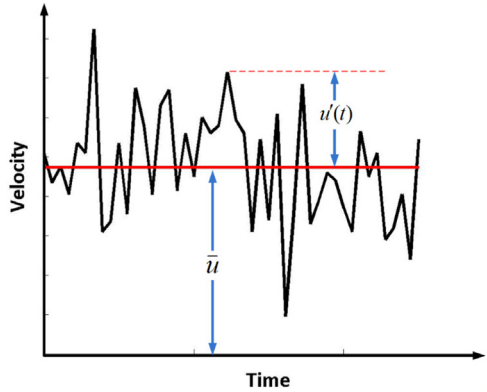


**Figure 3.2** Time variation of the horizontal velocity measured in turbulent flow.

to specific values when the averaging time is long enough, we can always write the instantaneous velocity, $\tilde{u}(t)$, as follows:

$$\tilde{u}(t) = U + u(t), \tag{3.3}$$

where $U$ is the time average or mean defined by

$$U = \underset{T\to\infty}{Lim}\ \frac{1}{T}\int_0^T \tilde{u}(t)dt, \tag{3.4}$$

and $u(t)$ is the fluctuating component. In our notation, upper case letters refer to mean quantities, and lower case refers to turbulent fluctuations. By convention, the horizontal components of the velocity are denoted by $u$ and $v$, and the vertical component by $w$.

The study of turbulence involves understanding the mean, and the statistics of the turbulent quantities under a variety of conditions. The statistic of greatest relevance to dispersion of pollution is the standard deviation of the fluctuating velocity defined by

$$\sigma_u = \left[\underset{T\to\infty}{Lim}\ \frac{1}{T}\int_0^T u^2 dt\right]^{1/2}. \tag{3.5}$$

Notice that, by definition, the time averages of the fluctuating quantities are zero. However, the average of the product of two fluctuating quantities is not zero.

Turbulence in the atmospheric boundary layer is generated by wind shear and buoyancy associated with sensible heating at the ground.

During the daytime, sensible heating at the surface results in parcels of air that are warmer, and hence less dense than their surroundings. These parcels are subject to buoyancy forces that accelerate them upward.

Turbulence in the boundary layer is also created by shear, which is the motion of a layer of air sliding past another layer with a different velocity. This leads to vertical turbulent motion that transfers momentum between these layers. This is essentially the mechanism that slows down the air as it flows past a stationary surface; momentum is transferred to the ground because the velocity increases with height near the ground.

The velocity time series, such as the one shown in Fig. 3.2, suggests that turbulent motion can be considered to consist of the superposition of the motion of turbulent "eddies" with a range of time and length scales. Turbulent energy is supplied by the mean flow, transferred from the large to the small eddies, and is ultimately dissipated through molecular viscosity at the smallest scales of motion.

In understanding the role of turbulence, it is useful to think of turbulent motion at a particular height in the boundary layer as dominated by an eddy with a length, $l$, and a velocity $w$. Then, its overturning timescale is $l/w$. The magnitude of the velocity scale in any particular direction is of the order of the standard deviation of the corresponding velocity fluctuations. The combination $wl$ is called the eddy diffusivity of turbulence, $K$. It turns out that under certain circumstances, the eddy diffusivity can be used to estimate the turbulent flux, $F_i$, of a quantity $\phi$ using the gradient formula $F_i = -K_i \frac{\partial \phi}{\partial x_i}$, where $i$ denotes a specific direction.

We can estimate the magnitude of the turbulent velocities generated by these two mechanisms, buoyancy and shear, using simple models.

## Convective Velocity Scale

As mentioned earlier, heat flux from the ground to the atmosphere creates buoyancy forces, which in turn generate turbulent velocities. We can estimate these turbulent velocities by considering an air parcel of unit mass that has a temperature excess of $\Delta T$ over its surroundings that it acquires at the heated ground. Taking the specific volume (volume per unit mass) of the parcel as $v$, the two forces on the parcel (neglecting drag forces for the moment) are

$$\text{Downward gravitational force} = g. \tag{3.6a}$$

$$\text{Upward buoyancy force} = vg\rho_s, \tag{3.6b}$$

where the subscript "$s$" refers to surroundings. Then, the net upward force is

$$F_u = \nu g \rho_s - g = g(\nu \rho_s - 1), \tag{3.7}$$

where $\rho_s$ is the density of the surroundings.

But

$$\nu = 1/\rho, \tag{3.8}$$

so that

$$F_u = g\left(\frac{\rho_s}{\rho} - 1\right) = g\left(\frac{T}{T_s} - 1\right) \text{ (from the gas law)} \tag{3.9}$$

or

$$F_u = g\frac{\Delta T}{T_s} \cong g\frac{\Delta \theta}{\theta_s}. \tag{3.10}$$

This force, acting over a distance $z$, generates a kinetic energy $\approx w^2$ so that

$$\frac{g\Delta\theta z}{\theta_s} \approx w^2. \tag{3.11}$$

Now let us multiply both sides of the equation by $w$,

$$\frac{g(\Delta\theta w)z}{\theta_s} \approx w^3. \tag{3.12}$$

The term inside the parentheses in Eq. (3.12) is the velocity of the parcel multiplied by the temperature excess carried by the parcel. This quantity is proportional to the surface heat flux:

$$\Delta\theta w \sim \frac{H}{\rho C_p}. \tag{3.13}$$

Then,

$$w \approx \left(\frac{g}{\theta_s}\frac{H}{\rho C_p} z\right)^{1/3}. \tag{3.14}$$

$H/\rho C_p$ is referred to as the kinematic heat flux, and is denoted by

$$\frac{H}{\rho C_p} = Q_0. \tag{3.15}$$

Now, define a *free convection scale*, $u_f$:

$$u_f = \left(\frac{g}{T_0} Q_0 z\right)^{1/3}. \tag{3.16}$$

where $T_0$ is the near surface temperature which is approximately equal to $\theta_s$ in a well-mixed convective boundary layer.

Another velocity scale that is used to characterize a boundary layer dominated by surface heating is the *convective velocity scale* given by

$$w_* = \left(\frac{g}{T_0} Q_0 z_i\right)^{1/3}, \tag{3.17}$$

where $z_i$ is the boundary layer height, which is also called the mixed layer because vertical motion induced by buoyancy leads to vigorous vertical mixing of the properties of the boundary layer.

## FRICTION VELOCITY

Except very close to the ground, the horizontal shear stress is supported by macroscopic turbulent motion. When parcels of air travel vertically, they exchange momentum between layers of air with different velocities. Vertical gradients in horizontal mean velocity lead to changes in instantaneous horizontal velocities during this transfer of momentum. If we denote the horizontal velocity fluctuation, $u'$, created by a parcel of air with vertical velocity, $w'$, the horizontal momentum transferred across a horizontal layer by the parcel is $\rho u'w'$, where $\rho$ is the air density. If the horizontal shear stress is roughly constant with height and is equal to the surface stress, $\tau_0$, then $\tau_0 = -\rho\overline{u'w'}$, where the overbar denotes a time average. The negative sign ensures that $\tau_0$ is positive because a positive $w'$ is associated with a negative $u'$ when the mean horizontal velocity increases with height. These arguments suggest that the turbulent velocities associated with shear production of turbulence scale with the surface friction velocity, $u_*$, defined by

$$u_* \equiv \sqrt{\frac{\tau_0}{\rho}}. \tag{3.18}$$

Buoyant and shear production of turbulence operate together to determine the structure of the boundary layer. A length scale, referred to

as the Monin–Obukhov length, allows us to combine the effects of these mechanisms into a single framework that describes the vertical structure of the near surface atmospheric boundary layer.

## MONIN–OBUKHOV LENGTH

The absolute value of the Monin–Obukhov length, $L$, is roughly the height at which the turbulent velocity generated by shear is equal to that produced by buoyancy:

$$u_* \sim u_f(z = L) = \left(\frac{g}{T_0} Q_0 L\right)^{1/3} \tag{3.19}$$

which yields the definition

$$L = -\frac{T_0 u_*^3}{gkQ_0}, \tag{3.20}$$

where the von Karman constant $k = 0.4$. The negative sign indicates that when $Q_0$ is positive during the day, $L$ is negative and positive when the heat flux is toward the ground. So $L$ is positive when the boundary layer is stable, and negative when it is unstable.

Notice from Eq. (3.16) that the velocity associated with buoyancy production of turbulence increases with height. On the other hand, the velocity associated with shear production is more or less constant in the surface layer. This allows us interpret the meaning of the Monin–Obukhov length, $L$. Shear production of turbulence dominates that by buoyancy at heights below the Monin–Obukhov length, while buoyant production becomes dominant above it.

### Surface Layer Similarity

At heights below the order of magnitude of the Monin–Obukhov length, the mean and the turbulent structure of the boundary layer can be described using Monin–Obukhov similarity theory (Businger, 1973). The theory states that the mean temperature and velocity gradients can be represented by universal functions if the velocity, temperature, and height are scaled appropriately. The velocity scale is $u_*$, the height scale is $L$, and the temperature scale, $\theta_*$, is given by

$$\theta_* = -\frac{Q_0}{u_*}. \tag{3.21}$$

Let us consider a neutral boundary layer, one that is dominated by shear. In such a boundary layer, the mean velocity gradient is of the same order as the velocity gradient across the dominant turbulent eddy at that height. We assume that the dominant eddy at a height $z$ has a length scale of order $z$ and a velocity scale of order $u_*$. Then, measurements indicate that we can write

$$\frac{dU}{dz} = \frac{u_*}{kz}, \tag{3.22}$$

where $k = 0.4$ is the von Karman constant. Integration yields the logarithmic expression for the mean wind speed at height $z$,

$$U(z) = \frac{u_*}{k}\ln\left(\frac{z}{z_0}\right), \tag{3.23}$$

where $z_0$ is the roughness length. The roughness length is related to the physical dimensions of the objects at the surface. Details on how this is estimated can be found in textbooks on micrometeorology, such as that by Stull (1988).

Monin–Obukhov Similarity theory states that we can account for the effects of heat flux by modifying Eq. (3.23) as follows:

$$\frac{dU}{dz} = \frac{u_*}{kz}\phi_m\left(\frac{z}{L}\right), \tag{3.24}$$

and the potential temperature gradient can be expressed as

$$\frac{d\theta}{dz} = \frac{\theta_*}{kz}\phi_h\left(\frac{z}{L}\right). \tag{3.25}$$

Notice that when the surface heat flux goes to zero, $L \to \infty$ and $z/L \to 0$. This means that $\phi_m(0) = 1$ and $\phi_h(0) = 1$ to be consistent with the gradient in the neutral boundary layer. Note that $\theta_*$ goes to zero when the surface heat flux goes to zero.

The forms represented by Eqs. (3.24) and (3.25) are well supported by observations (Businger et al., 1971), which indicate that

$$\phi_m = \left(1 - 15\frac{z}{L}\right)^{-1/4} \text{ for } L < 0, \tag{3.26a}$$

$$= 1 + 4.7\frac{z}{L} \text{ for } L > 0, \tag{3.26b}$$

and

$$\phi_h = 0.74\left(1 - 9\frac{z}{L}\right)^{-1/2} \text{ for } L < 0, \tag{3.27a}$$

$$= 0.74 + 4.7\frac{z}{L} \text{ for } L > 0. \tag{3.27b}$$

With these forms for $\phi_m$ and $\phi_h$, Eqs. (3.24) and (3.25) can be integrated to yield

$$\frac{U}{u_*} = \frac{1}{k}\left(\ln\frac{z}{z_0} - \psi_1\left(\frac{z}{L}\right) + \psi_1\left(\frac{z_0}{L}\right)\right), \text{ for } L < 0, \tag{3.28a}$$

where

$$\psi_1 = 2\ln\left[\frac{(1+x)}{2}\right] + \ln\left[\frac{(1+x^2)}{2}\right] - 2\tan^{-1}x + \frac{\pi}{2} \tag{3.28b}$$

and

$$x = \left(1 - 15\frac{z}{L}\right)^{1/4}. \tag{3.28c}$$

For stable conditions, $(L > 0)$,

$$\frac{U}{u_*} = \frac{1}{k}\left\{\ln\left(\frac{z}{z_0}\right) + 4.7\frac{(z - z_0)}{L}\right\}. \tag{3.29}$$

The expressions for temperature are as follows.

Unstable conditions, $L < 0$

$$\frac{\theta - \theta_o}{\theta_*} = 0.74/k\left[\ln\left(\frac{z}{z_o}\right) - \psi_2\left(\frac{z}{L}\right) + \psi_2\left(\frac{z_0}{L}\right)\right], \tag{3.30}$$

where

$$\psi_2 = \ln\left[\frac{(1+\gamma)}{2}\right], \tag{3.30a}$$

and

$$\gamma = \left(1 - 9\frac{z}{L}\right)^{1/2}. \tag{3.30b}$$

Stable conditions, $L > 0$

$$\frac{\theta - \theta_0}{\theta_*} = 0.74/k\left\{\ln\left(\frac{z}{z_0}\right) + 4.7\frac{(z - z_0)}{L}\right\}. \tag{3.31}$$

In these expressions for the temperature profiles, $\theta_0$ represents the temperature obtained by extrapolating the profile to $z = 0$; this is not the surface temperature. In principle, these profiles can be used to compute surface fluxes of heat and momentum by fitting them to temperature and velocity measurements.

The following sections explain the structures of the upper part of the daytime and nighttime boundary layers.

## THE DAYTIME BOUNDARY LAYER

Turbulence in the daytime boundary layer is maintained primarily by sensible heating at the surface, which results in parcels of air that are warmer than their surroundings. These parcels are subject to buoyancy forces that accelerate them upward. The mixing induced by these parcels gives rise to the boundary layer or mixed layer, whose growth is inhibited by the stable temperature gradient of the atmosphere above the mixed layer. Often, the growth of the mixed layer is limited by a sharp subsidence inversion or temperature jump, in which case the height of this inversion determines the maximum mixed layer height.

The turbulent motion in the convective boundary layer is organized into long-lived updrafts and downdrafts that extend through the depth of the boundary layer. These structures are carried by the mean wind as illustrated in Fig. 3.3.

The updrafts consist of accelerating parcels, while the downdrafts are caused by compensating downward motion. Thus, the velocities in updrafts are higher than those in downdrafts; mass balance requires that the horizontal area occupied by downdrafts is higher than that of updrafts. This feature has important effects on dispersion from elevated stacks. Because more material is released into downdrafts than updrafts, the plume centerline descends toward the ground. This gives rise to a vertical concentration distribution that cannot be described with a Gaussian.

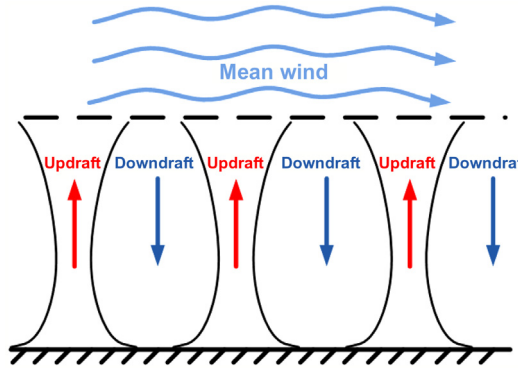


**Figure 3.3** Schematic of updrafts and downdrafts caused by surface heating.

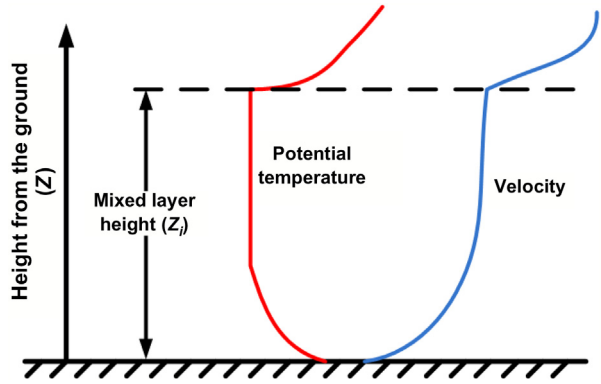


**Figure 3.4** Schematic of vertical profile of potential temperature and velocity in the convective boundary layer.

The mean potential temperature and velocity structure in an idealized mixed layer are shown in Fig. 3.4.

The potential temperature is super-adiabatic close to the surface: the potential temperature decreases with height. Above a tenth of the mixed layer height, the potential temperature is relatively uniform because of vigorous vertical mixing. The mixed layer is usually capped by a sharp inversion, especially in areas such as Los Angeles, where semipermanent high-pressure regions create strong subsidence inversions. This inversion limits the height of the mixed layer by resisting the vertical motion of thermals in the mixed layer. The layer above the mixed layer can be stably stratified.

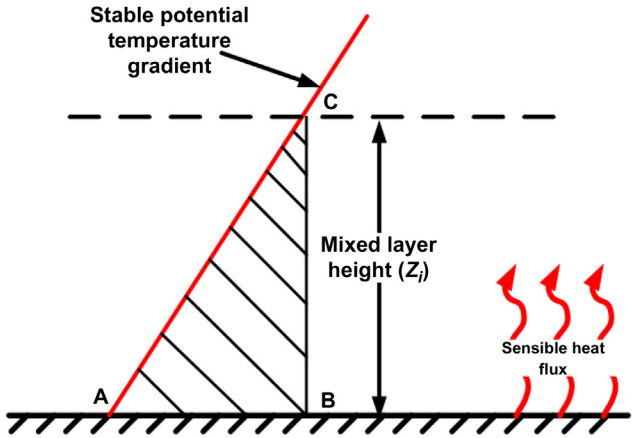


**Figure 3.5** Schematic for the calculation of convective boundary layer height.

The velocity profile in the daytime boundary layer is relatively flat in the mixed layer. The rapid change in velocity at the top of the boundary layer reflects the fact that the velocity is vertically mixed below the top.

## Height of the Convective Boundary Layer

The height of the mixed layer can be estimated by assuming that the sensible heat input into the atmosphere is used to modify the potential temperature in the mixed layer. Recall from Chapter 2 that the potential temperature, $\theta$, can be used to measure energy changes in the boundary layer; the potential temperature of a parcel changes in response to heat input.

Consider a mixed layer that grows by eroding a layer with a stable potential temperature gradient, as shown in Fig. 3.5.

Assume that the initial temperature profile is represented by AC. Then BC represents the potential temperature after sensible heating has occurred over a time, $T$, since sunrise. Then, AB is the temperature change at the surface, and the triangle ABC represents the modification of the energy of the atmospheric boundary layer. Denoting the potential temperature gradient of AC by $\gamma$, and the temperature change AB by $\Delta\theta$, the energy equivalent of the triangle ABC can be written as

$$\textit{Energy} \text{ in ABC} = \rho C_p \frac{1}{2} \Delta\theta z_i. \tag{3.32}$$

Noticing that $\Delta\theta = \gamma z_i$, we can equate this energy to the sensible heat flux integrated over $T$ to obtain

$$\rho C_p \frac{1}{2}\gamma z_i^2 = \int_0^T H(t)dt, \tag{3.33}$$

where $H(t)$ is the time-varying sensible heat flux. For simplicity, if we assume that the sensible heat flux increases linearly with time, we obtain the following expression for the mixed layer height:

$$z_i^2 = \frac{H_{\max} T}{\gamma \rho C_p}, \tag{3.34}$$

where $H_{\max}$ is the maximum heat flux. If we assume that the maximum occurs at noon, Eq. (3.34) can be used to estimate $z_i$ at noon. Taking $H_{\max}/\rho C_p = 0.3$ m/sK, $T = 6$ hours, and $\gamma = 5$ K/1000 m, we find $z_i \sim 1000m$. Note that the boundary layer height increases with time as long as the heat flux is positive. So the maximum height occurs at sunset. Assuming that this occurs 6 hours after noon, we see from Eq. (3.34) that its value is about $\sqrt{2} \times 1000 = 1414$m.

It was shown earlier that the turbulent velocities generated by buoyancy in the surface layer are proportional to the free convection velocity scale, $u_f$ defined by

$$u_f = \left(\frac{g}{T_s} Q_0 z\right)^{1/3}. \tag{3.35}$$

For heights below $0.1z_i$ we find that buoyancy generates velocities given by

$$\sigma_w = 1.3u_f; \quad z \leq 0.1z_i. \tag{3.36}$$

We saw earlier that at heights less than $|L|$, where turbulence production is dominated by shear, $\sigma_w$ is roughly proportional to $u_*$,

$$\sigma_w = 1.3u_*. \tag{3.37}$$

A formulation for $\sigma_w$ that interpolates between the limits set by $1.3u_*$ and $u_f$ is given by Panofsky et al. (1977) as

$$\sigma_w = 1.3\left(u_*^3 + u_f^3\right)^{1/3}, \tag{3.38}$$

yielding

$$\frac{\sigma_w}{u_*} = 1.3\left[1+2.5\left(\frac{-z}{L}\right)\right]^{1/3}. \tag{3.39}$$

Between $0.1z_i$ and close to the top of the mixed layer, $\sigma_w$ associated with buoyancy production of turbulence is proportional to the convective velocity scale given by

$$w_* = \left(\frac{g}{T_s} Q_0 z_i\right)^{1/3}, \tag{3.40}$$

where $z_i$ is the mixed layer height. Then, we find that

$$\sigma_w = \sigma_v = \sigma_u \cong 0.6 w_*. \tag{3.41}$$

It is found that $\sigma_u$ and $\sigma_v$ are also proportional to $w_*$, even below $0.1z_i$. The shear contribution to the turbulence levels is usually small relative to the buoyancy contribution at heights above $0.1z_i$.

## THE NIGHTTIME BOUNDARY LAYER

When the sun sets, turbulence energy production by buoyancy comes to a stop. Over a period of an hour, the turbulence in the mixed layer collapses, and shear becomes the primary mechanism for the production of turbulence. Because the ground is initially warmer than the atmosphere, the thermal radiation leaving the ground exceeds that being supplied by the atmosphere. This deficit leads to a cooling of the ground.

Initially, both the sensible heat flux and the ground heat flux are directed away from the earth's surface. The surface cools rapidly, and a point is reached at which the ground becomes colder than the layers above in the atmosphere. At this stage, the heat flux from the atmosphere is directed toward the earth's surface. This process is referred to as the formation of a radiation-induced surface inversion—the temperature (and the potential temperature) increases with height.

The mean temperature and velocity above the surface boundary layer increase with height as shown in Fig. 3.6.

There is little agreement on the general form of these profiles in the stable boundary layer. On the basis of measurements made in Holland,

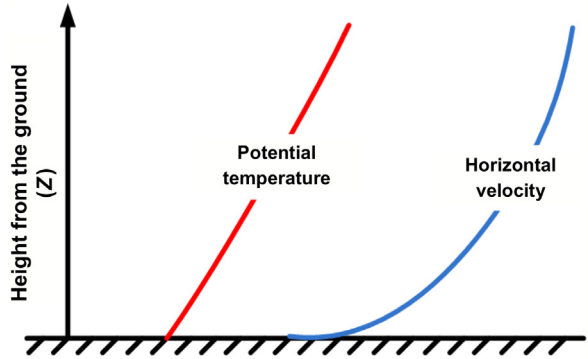


**Figure 3.6** Schematic of vertical profile of potential temperature and velocity in the stable boundary layer.

Van Ulden and Holtslag (1985) suggest that the mean wind can be described by

$$u(z) = \frac{u_*}{k}\left[\ln\left(\frac{z}{z_o}\right) - \psi_m\left(\frac{z}{L}\right) + \psi_m\left(\frac{z_o}{L}\right)\right] \tag{3.42}$$

where

$$\psi_m\left(\frac{z}{L}\right) = -17\left[1 - \exp\left(-0.29\frac{z}{L}\right)\right]$$

The horizontal wind usually shows considerable turning with height. Van Ulden and Holtslag (1985) propose the following equation to estimate this turning:

$$\frac{D(z)}{D(z_i)} = d_1\left[1 - \exp\left(-d_2\frac{z}{z_i}\right)\right] \tag{3.43}$$

where

$$d_1 = 1.58;\ d_2 = 1.0$$

and

$$D(z_i) \cong 35^\circ$$

Here $z_i$ is the height of the boundary layer, which is discussed later. We do not have similar equations for the variation of temperature through the depth of the boundary layer. In the absence of information through measurements, we suggest extrapolating the surface boundary layer, Eq. (3.30), through the boundary layer.

Most expressions for the height of the stable boundary layer, which we denote by $h$, are based on dimensional analysis backed by relatively weak physical arguments. One scheme assumes

$$\frac{dh^2}{dt} \sim wl, \tag{3.44}$$

where $l$ is the length scale and $w$ is the velocity scale of the turbulent eddies leading to the growth of the boundary layer. The combination $wl$ is called the eddy diffusivity of turbulence, $K$. We will see later how $K$ can be used to derive useful formulas for dispersion of pollutants.

If we assume that the turbulent eddies in the stable boundary layer scale with the Monin−Obukhov length, $L$, $K$ can be written as

$$K \sim u_* L, \tag{3.45}$$

where $u_*$ is the surface friction velocity. If $L$ exceeds $h$, the eddies scale with $h$, and $K$ is written as

$$K \sim u_* h. \tag{3.46}$$

Thus, when $h$ is small relative to $L$, substituting Eq. (3.46) into Eq. (3.44) yields

$$\frac{dh}{dt} = \alpha u_*, \tag{3.47}$$

where $\alpha$ is a constant that needs to be determined empirically.

When $h$ exceeds $L$, Eqs. (3.45) and (3.44) give

$$\frac{dh^2}{dt} \sim u_* L. \tag{3.48}$$

We can obtain Zilitinkevich's expression for the stable boundary layer height by integrating Eq. (3.48) assuming that $u_*$ and $L$ are constant:

$$h^2 \sim u_* L t, \tag{3.49}$$

and taking the time of growth, $t$, to be governed by the Coriolis parameter, $f$, as follows:

$$t = 1/f. \tag{3.50}$$

Then,

$$h = a\left(\frac{u_* L}{f}\right)^{1/2}, \tag{3.51}$$

where $a$ is an empirically determined constant.

We can readily write an expression that varies continuously between Eqs. (3.47) and (3.48) (for constant $u_*$ and $L$) as follows:

$$h = u_* t \left[ \frac{L/h}{a + bL/h} \right]. \tag{3.52}$$

Eq. (3.52) reduces to Nieuwstadt's (1981) interpretation if we put $t = 1/f$.

The problem with diagnostic equations such as Eq. (3.52) is that the height of the boundary layer reacts instantaneously to $u_*$ and $L$. This means that $h$ will drop suddenly (and unrealistically) if the wind speed, and thus $u_*$, decreases quickly. One way of getting around this problem is to allow the boundary layer to have some inertia. This is done by using the following equation to estimate the time evolution of $h$:

$$\frac{dh}{dt} = \frac{h_d - h}{\tau}, \tag{3.53}$$

where $h_d$ is the estimate given by the diagnostic equation, and $\tau$ is the timescale, given by

$$\tau = \frac{\beta h}{u_*}, \tag{3.54}$$

where $\beta$ is an empirical constant.

When $h_d = h$, $h$ does not change. If $h_d$ increases suddenly in response to an increase in wind speed, $dh/dt$ becomes positive, so that $h$ will grow toward $h_d$; the time of reaction is proportional to $h/u_*$. This means that if either $h$ is large, or $u_*$ is small, $h$ reacts slowly to changes in $h_d$. It is seen that sudden decreases in $h_d$ do not result in similar changes in $h$ unless the reaction timescale, $\tau$, is small enough.

One way of interpreting Eq. (3.54) is to think of $h_d$ as the input to a system, while $h$ is the required output. The response of $h$ to changes in $h_d$ is damped by the timescale, $\tau$. If $\tau$ is large, $h$ responds slowly to changes in $h_d$; a small $\tau$ allows $h$ to follow changes in $h_d$.

## Turbulent Velocities in the Stable Boundary Layer

As explained earlier, the stable potential temperature gradient suppresses the production of turbulence because it opposes vertical motion. Under these circumstances, shear production of turbulence is matched by the

destruction associated with the stable temperature gradient and viscous dissipation. This balance between these processes of production and turbulence leads to relatively small levels of turbulence in the nocturnal boundary layer. The low turbulence levels in the stable boundary layer are accompanied by smaller dispersion rates compared to those in the daytime atmospheric boundary layer. Elevated plumes show little vertical spread during the night because of the low levels of turbulence.

The presence of clouds increases the thermal radiation reaching the earth's surface. The surface cools less under these circumstances, and the nocturnal inversion is less pronounced. This implies that turbulence levels in cloudy conditions are higher than those found under cloud-free conditions. This effect of clouds is substantially different from that during the day, when clouds decrease the solar radiation reaching the ground. During daytime when clouds are present, turbulence levels, associated with buoyancy production of turbulence, are reduced compared to those under clear sky conditions.

While we do know that the levels of turbulence in the stable boundary layer are low, we are not in a good position to characterize the variation of these levels as a function of height. The parameterization that is sometimes used to estimate $\sigma_w$ is that of Nieuwstadt (1984):

$$\sigma_w^2 = 1.7u_*^2\left(1 - \frac{z}{h}\right). \tag{3.55}$$

We point out that the observational evidence to support Eq. (3.55) is meager; measurements indicate that $\sigma_w$ can actually increase with height. Under these circumstances, it is advisable to use measurements when possible.

The horizontal turbulent velocities, $\sigma_u$ and $\sigma_v$, in the stable boundary layer do not appear to be related to micrometeorological variables. They are affected by mesoscale flows and local topography, which are difficult to characterize using models. In the absence of measurements, a value of $\sigma_v$ of 1 m/s can be used.

The following sections describe the application of the micrometeorology to estimating dispersion in the surface atmospheric boundary layer.

## Dispersion Modeling—Ground-Level Source

The concepts that underlie the formulation of a dispersion model can be illustrated by constructing a simple model to estimate ground-level concentrations associated with a surface release. This type of model is relevant for pollution related to transportation because vehicle emissions occur

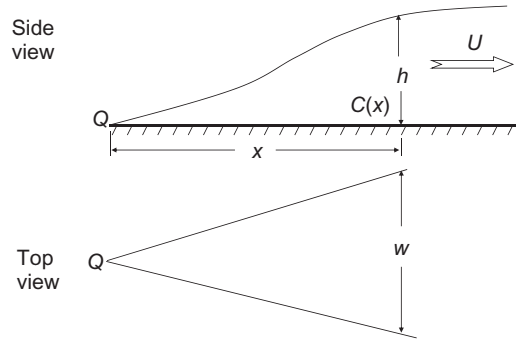


**Figure 3.7** Schematic of plume dispersion from a surface release.

close to the ground. Fig. 3.7 shows a plume originating from a point source close to the ground. The plume outline represents a time average so that the irregular boundaries of the observed instantaneous plumes are smoothed out through time exposure. The concentrations associated with an instantaneous plume are difficult to estimate, while a time-averaged plume is more amenable to analysis.

Assume that pollutant release rate (mass/time) is $Q$. For simplicity, we take the pollutant to be well mixed both in the horizontal and the vertical through the cross-sectional area of the plume. At a distance, $x$, from the source, the cross-sectional area is the height, $h$, multiplied by the width, $w$. Then, the material passing through this area is $C(x)hwU$, where the wind speed, $U$, is taken to be constant over the height of the plume. If we assume that no material is removed by the ground, the emission rate, $Q$, has to be equal to the transport of material through the plume cross section at any distance. This yields the following expression for the concentration, $C(x)$,

$$C(x) = \frac{Q}{Uhw}. \tag{3.56}$$

Although this is a highly simplified model of the real world, it contains the essentials of dispersion models used in regulatory applications. In fact, Eq. (3.56) multiplied by a constant was the basis of the dispersion scheme proposed by Pasquill in 1961.

How do we determine the height and width of a plume when, in reality, the concentration is not uniform across the cross section of the plume? Observations indicate that the time-averaged concentration distribution is approximately Gaussian in the horizontal. The distribution in

the vertical is not Gaussian, as we will see later, but most models assume that this distribution holds in the vertical as well. Notice that the actual concentration measurements might deviate significantly from the smooth Gaussian curve.

The models described in this chapter are designed to estimate concentrations averaged over an hour. They cannot be used to estimate instantaneous concentrations, which are relevant to odor. This chapter also provides the background necessary to understand the approach used in the formulation of such models. This includes the essentials of the micrometeorology used to construct the inputs for the model.

## THE POINT SOURCE IN THE ATMOSPHERIC BOUNDARY LAYER

Models to estimate the impact of vehicle emissions are based on the framework of the steady-state Gaussian dispersion equation. If the release point is taken to be the origin ($z = 0$), with the $x$-axis of the coordinate system aligned along the wind direction at the source, the time-averaged (typically 1 hour) concentration field is described in terms of the Gaussian distribution (see Fig. 3.8):

$$C(x, y, z) = \frac{Q}{2\pi\sigma_y\sigma_z U} exp\left[-\frac{z^2}{2\sigma_z^2} - \frac{y^2}{2\sigma_y^2}\right], \tag{3.57}$$

where $y$ is the distance from the plume centerline, shown as a dotted line in Fig. 3.8, and $\sigma_y$ is the standard deviation of the horizontal Gaussian

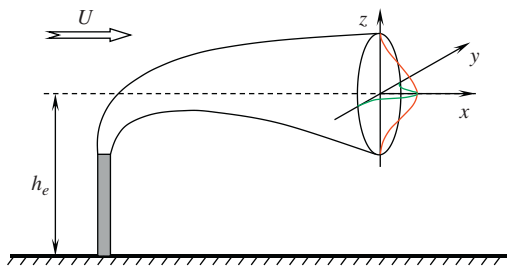


**Figure 3.8** Gaussian distribution used to model the plume from a point source. For the time being, we have ignored the effects of the impermeable ground on the concentration field.

distribution. The second exponential in the equation describes the vertical distribution, where $z$ is the height measured from the release point, and $\sigma_z$ is the standard deviation of the vertical Gaussian distribution. The standard deviations of the distributions, $\sigma_y$ and $\sigma_z$, are referred as the horizontal and vertical spreads of the plume, respectively. $Q$ is the source strength (mass/time), and $U$ is the time-averaged wind speed at source height.

Eq. (3.57) assumes that along-wind dispersion is much smaller than transport by the mean wind. This assumption breaks down when the mean wind is comparable to the turbulent velocity along the mean wind direction, $\sigma_u$.

The effect of the ground on concentrations is accounted for by making sure that there is no flux of material through the ground, which we now take to be $z = 0$. The mathematical trick to achieve this is to place an "image" source at a distance $z = -h_e$, where $h_e$ is the effective height of the source above ground. The upward flux from this image source essentially cancels out the downward flux from the real source without affecting the mass balance. Then, the concentration becomes

$$C(x, y, z) = \frac{Q}{2\pi\sigma_y\sigma_z U} exp\left[-\frac{y^2}{2\sigma_y^2}\right]\left\{exp\left[-\frac{(z-h_e)^2}{2\sigma_z^2}\right] + exp\left[-\frac{(z+h_e)^2}{2\sigma_z^2}\right]\right\}. \tag{3.58}$$

In the real atmosphere, dispersion in the upward direction is limited by the height of the atmospheric boundary layer. This limitation of vertical mixing is incorporated into the Gaussian formulation by "reflecting" material off the top of the mixed layer. Then, Eq. (3.58) can be modified to account for the infinite set of "reflections" from the ground and the top of the mixed layer.

The Gaussian formulation for a point source can be used to model both volume and point sources because each of these source types can be discretized into point sources; the associated concentrations are simply the sums of the contributions from these point sources.

## DISPERSION IN THE ATMOSPHERIC BOUNDARY LAYER

Until recently plume spread formulations were based on those derived empirically by Pasquill (1961) in the 1960s from observations made during the Prairie Grass dispersion experiment conducted in

Nebraska in 1956 (Barad, 1958). These formulations were modified subsequently by Gifford and Turner, and are commonly referred to as the Pasquill–Gifford–Turner (PGT) curves. For dispersion in urban areas, the Industrial Source Control (ISC) model uses the McElroy–Pooler curves that are derived from experiments conducted in St. Louis, Missouri (McElroy and Pooler, 1968).

The dispersion curves are keyed to stability classes that are related to ranges in the wind speed and incoming solar radiation. The wind speed, measured at 10 m above ground level, is an indicator of turbulence produced by shear, while the incoming solar radiation is a surrogate for the sensible heat flux, which generates turbulence. Thus, the stability classes contain information on shear and buoyancy produced turbulence.

Classes A, B, and C correspond to unstable conditions when buoyancy production of turbulence adds to that due to shear. The sensible heat flux under these conditions is upward. Class A, the most unstable, is associated with the most rapid dispersion rates; the plume spreads for a given distance decreases as we go from class A to C. Class D corresponds to neutral conditions when turbulence production is dominated by shear. Classes E and F are associated with stable conditions. Class F corresponds to the lowest dispersion rates. Thus six dispersion curves, which are only functions of distance from the source, are used to describe the entire range of possible dispersion conditions.

The major advantage of the PGT curves is that they are based on observations and thus provide realistic concentration estimates under a variety of meteorological conditions. Their shortcoming is that they are derived from dispersion of surface releases and are thus not applicable to elevated releases. Furthermore, their formulation does not allow the use of on-site turbulence levels to describe dispersion more accurately than the "broad brush" PGT curves.

In the more recently formulated models such as AMS EPA Regulatory Model (AERMOD) (Cimorelli et al., 2005), plume spreads are described using the solution of the species conservation equation. It turns out that we can learn a great deal about dispersion in the near surface boundary layer using the mass conservation equation expressed in terms of the crosswind-integrated concentration, $\overline{C}^{y}$, which we denote by $C$ here for convenience:

$$U(z)\frac{\partial C}{\partial x} = \frac{\partial}{\partial z}\left(K(z)\frac{\partial C}{\partial z}\right), \tag{3.59}$$

where $K(z)$ is the vertical eddy diffusivity and $U(z)$ is the horizontal velocity. We take the source, with emission rate $Q$ (mass/(time/length)), to be located at ground level at $x = 0$. We assume that there is no flux at the surface and top of the domain and thus the vertical concentration gradients are $\frac{\partial C}{\partial z} = 0$, at $z = 0$ and $z = \infty$, which implies no deposition at the surface. The eddy diffusivity concept, which is based on an analogy with molecular transport, cannot be justified rigorously for turbulent transport. However, it has heuristic value and is useful for developing semiempirical models of turbulent transport.

It can be shown that the eddy diffusivity concept is most applicable when the scale of concentration variation, the plume spread, is larger than the scale of the eddies responsible for plume spreading. In the surface boundary layer, plume spread in the vertical direction is comparable to the length scale of the eddies responsible for vertical transport. It turns out that the eddy diffusivity concept is useful in the surface boundary layer, where Monin−Obukhov similarity provides useful relationships between velocity and temperature gradients and the corresponding heat and momentum fluxes. These relationships can be used to derive eddy diffusivities for heat and momentum, which can be used to describe dispersion by evaluating them at some fraction of the plume height.

Most currently used dispersion models are based on the theoretical foundations laid by a group of workers who showed that understanding of surface micrometeorology, gained in the 1970s, could be used to construct models for dispersion in the surface layer. Several approaches have been in formulating these models. We will follow that proposed by Van Ulden (1978) because it is relatively straightforward.

We can obtain a useful analytical solution of Eq. (3.59) for the following forms of $U(z)$ and $K(z)$:

$$U(z) = U_1 z^m \quad K(z) = K_1 z^n. \tag{3.60}$$

The solution is

$$\frac{C}{Q} = \frac{p}{U_1 \Gamma(s)} \left(\frac{b}{x}\right)^s \exp\left(-\frac{b z^p}{x}\right), \tag{3.61}$$

where

$$\begin{aligned} b &= \frac{U_1}{K_1 p^2} \quad p = m - n + 2 \\ s &= \frac{m+1}{p} \end{aligned}, \tag{3.62}$$

and $\Gamma(s)$ is the gamma function defined by $\Gamma(x) = \int_0^\infty t^{x-1}\exp(-t)dt$.

Because the eddy diffusivity equation is a useful model for surface layer dispersion, the solution provides insight into the behavior of crosswind-integrated concentrations under different stabilities. The first thing to notice is that $p$, the exponent of $z$, depends on the exponents $m$ and $n$, which means that the vertical distribution is not Gaussian. That is, $p$ does not equal 2 as elementary dispersion models assume.

In the neutral boundary layer $K = ku_*z$ so that $n = 1$, which means that for any value of $m$, $s = 1$. This means that the crosswind-integrated concentration falls of as $1/x$, where $x$ is the distance from the source. This means that the concentration from a long line source falls off approximately as distance from the source, as we saw earlier.

When the boundary layer is very stable, $U \sim u_*z/L$ and $K \sim u_*L$ so that $m = 1$ and $n = 0$. This means that $p = 3$, and $s = 2/3$. Notice that for this asymptotic condition, the concentration falls much more rapidly with increasing height than for the value $p = 2$ corresponding to the Gaussian profile. The crosswind-integrated concentration (concentration associated with a line source) falls of as $1/x^{2/3}$.

Under very unstable conditions, the wind speed varies little with height, so that $m = 0$. If we assume that the eddy diffusivity corresponds to that for heat, $K \sim z^{3/2}$, so that $n = 3/2$. Then, $p = 1/2$ and $s = 2$. So the vertical concentration falls of much less rapidly than the Gaussian $p = 2$, and the crosswind-integrated concentration falls of as $1/x^2$.

Van Ulden (1978) shows that we can adapt this solution for any form of the wind speed and eddy diffusivity by recasting the solution, Eq. (3.61), in terms of the mean wind speed, $\overline{U}$, and mean plume height, $\overline{z}$, defined by

$$\overline{U} = \frac{\int_0^\infty U(z)C(z)dz}{\int_0^\infty C(z)dz}$$
$$\overline{z} = \frac{\int_0^\infty zC(z)dz}{\int_0^\infty C(z)dz} \quad . \tag{3.63}$$

Then, Eq. (3.61) can be rewritten as

$$\frac{C}{Q} = \frac{S}{\overline{U}\overline{z}} \exp\left(-\left(\frac{Bz}{\overline{z}}\right)^{p}\right), \tag{3.64}$$

where

$$S = \frac{p\Gamma(2/p)}{\left[\Gamma(1/p)\right]^2} \quad B = \frac{\Gamma(2/p)}{\Gamma(1/p)}. \tag{3.65}$$

This solution becomes useful with the accompanying equation for $\overline{z}$ obtained by differentiating the expression in Eq. (3.63).

$$\frac{d\overline{z}}{dx} = \frac{K(q\overline{z})}{U(q\overline{z})q\overline{z}} \qquad q = (B^p p)^{\frac{1}{1-p}}. \tag{3.66}$$

Van Ulden(1978) shows that for neutral and unstable conditions,

$$\overline{U} = U(0.6\overline{z}) \tag{3.67}$$

is a useful approximation. And for stable conditions,

$$\overline{U} = \frac{u_*}{k}\left[\ln\left(\frac{0.6\overline{z}}{z_0}\right) + 4.7\frac{\overline{z}}{L}\right]. \tag{3.68}$$

By using a constant value for $q = 1.55$ based on $p = 1.5$, Van Ulden (1978) derives implicit expressions for $\overline{z}$ in terms of $z_0$ and $L$. More explicit forms of $\overline{z}$ expressed in terms of $\sigma_z$ are presented in the bulk of the chapter.

Van Ulden (1978) shows that the analytical solution presented in Eqs. (3.64)–(3.68) provides an excellent description of ground-level concentrations measured in Prairie Grass (Barad, 1958). By assuming that the profiles of velocity and eddy diffusivity can be approximated with power laws, Gryning et al. (1983) show that useful estimates of the exponent $p$ of $z$ in the vertical concentration distribution can be obtained from

$$m = \frac{z}{U}\frac{\partial U}{\partial z} \quad n = \frac{z}{K_h}\frac{\partial K_h}{\partial z}, \qquad p = m - n + 2 \tag{3.69}$$

resulting in

$$p = \frac{1+2\beta\zeta}{1+\beta\zeta} + \frac{1+\beta\zeta}{\ln\left(\frac{z_r}{z_0}\right)+\beta\zeta} \quad \zeta > 0$$
$$p = \frac{1-4.5\zeta}{1-9\zeta} + \frac{(1-15\zeta)^{-1/4}}{\ln\left(\frac{z_r}{z_0}\right)-\psi_m(\zeta)} \quad \zeta < 0 \qquad (3.70)$$

where $\zeta = \left(z_r/L\right)$, $z_r = 0.8\overline{z}$ for stable conditions and $z_r = 0.4\overline{z}$ for unstable conditions. The function $\psi_m(\zeta)$ corresponds to the Businger–Dyer expression in the velocity distribution

$$\psi_m = 2\ln\left(\frac{1+x}{2}\right) + \ln\left(\frac{1+x^2}{2}\right) - \tan^{-1}x + \frac{\pi}{2}. \qquad (3.71)$$
$$x = (1-15\zeta)^{1/4}$$

We can evaluate the usefulness of these formulas through the numerical solution of Eq. (3.59) using the Businger–Dyer expressions for the wind speed, $U(z)$, and eddy diffusivity, $K_h(z)$. Fig. 3.9 compares the ground-level concentrations obtained from the numerical solution with the Prairie

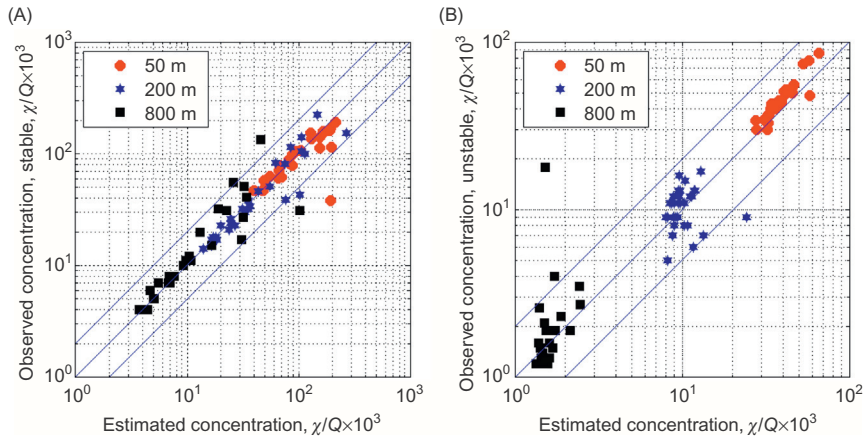


**Figure 3.9** Comparison of estimates of crosswind integrated ground-level concentrations from numerical model with corresponding observations from Prairie Grass: (A) stable conditions and (B) unstable conditions. The legend refers to distance from the source. Source: *Data obtained from Van Ulden, A.P., 1978. Simple estimates for vertical dispersion from sources near the ground. Atmos. Environ. 12, 2125–2129.*

Grass data presented by Van Ulden (1978). The deposition velocity of the tracer, $SO_2$, used in the experiment is taken to be $v_d = 0.07u_*$.

The comparison is good although there is scatter during unstable conditions at 200 and 800 m. Nieuwstadt and Van Ulden (1978) showed that the numerical solution provides an adequate description of the vertical concentration distribution measured at towers located 100 m from the source in the Prairie Grass experiment. They find that the vertical distribution is described well by the solution of:

$$C(x,z) = C(x,0)\exp(-\beta z^p), \tag{3.72}$$

where $\beta$ and $p$ are obtained through a fitting procedure. It turns out that $p = 2$, corresponding to the Gaussian distribution, is appropriate only under very stable conditions. Under unstable conditions, $p$ is usually less than one. The model, given by Eq. (3.70), provides an adequate description of the magnitude as well as the trend of $p$ as a function of $\overline{z}/|L|$.

The plume spreads, $\sigma_z$, formulated in the last section assumed that the vertical distribution is Gaussian. This error is not significant in computing the ground-level concentration because the empirical constants in the formulations reflect the variation of $p$ with stability. However, the error is important in computing the vertical distribution of concentrations. Because the vertical distribution can be approximated with Eq. (3.64), the expression for the crosswind integrated concentration becomes

$$\frac{C(x,z)}{Q} = \sqrt{\frac{2}{\pi}}\frac{1}{\overline{U}\sigma_z}\exp\left(-D\left(\frac{z}{\sigma_z}\right)^p\right)$$

where

$$D = \left[\sqrt{\frac{2}{\pi}}\frac{\Gamma(1/p)}{p}\right]^p . \tag{3.73}$$

Note that $\sigma_z$ requires an iterative calculation because, the mean velocity, $\overline{U}$, depends on $\overline{z}$, which in turn is related to $\sigma_z$ through

$$\overline{z} = \sigma_z\left(\sqrt{\frac{\pi}{2}}\frac{p\Gamma(2/p)}{\left[\Gamma(1/p)\right]^2}\right). \tag{3.74}$$

## Plume Spread Formulation Used in Current Models

We can formulate expressions for plume spreads of near surface releases by writing Eq. (3.66) as

$$U\frac{d\sigma_z^2}{dx} \sim K(\alpha\sigma_z), \tag{3.75}$$

where $\alpha$ is a constant and because $\overline{z} \sim \sigma_z$ for ground-level releases. We take $K$, the eddy diffusivity, to correspond to that of heat given by

$$K_H = \frac{u_*\theta_*}{d\theta/dz} = \frac{ku_*z}{\phi_H\left(\frac{z}{L}\right)}, \tag{3.76}$$

where

$$\frac{d\theta}{dz} = \frac{\theta_*}{kz}\phi_H\left(\frac{z}{L}\right), \tag{3.77}$$

where $\phi_H(\frac{z}{L})$ is the Monin−Obukhov similarity function and $L$ is the Monin−Obukhov length.

Let us first consider the near neutral boundary layer in which $\phi_H = 1$, so that $K_H \sim u_*z$. In applying Eq. (3.75) we assume that the eddy diffusivity and the wind speed correspond to a height that is a fraction of $\sigma_z$ so that

$$\begin{aligned} \sigma_z\frac{d\sigma_z}{dx} &\sim \frac{u_*\sigma_z}{U(\sigma_z)} \\ \frac{d\sigma_z}{dx} &\sim \frac{u_*}{U(\sigma_z)} \end{aligned}. \tag{3.78}$$

Now, the effective wind speed is given by the neutral expression

$$U(\sigma_z) \sim u_*\ln\left(\frac{\sigma_z}{z_0}\right), \tag{3.79}$$

which when substituted in Eq. (3.78) and integrated yields

$$\sigma_z\left[\ln(\sigma_z/z_0) - 1\right] + z_0 \sim x, \tag{3.80}$$

We can replace the logarithmic term in Eq. (3.80) to obtain

$$\sigma_z\left[\frac{U}{u_*} - 1\right] + z_0 \sim x. \tag{3.81}$$

Now $u_*$ is usually a small fraction of $U$ except at small distances from the source. Thus, Eq. (3.81) can be approximated by

$$\sigma_z U \sim u_* x. \tag{3.82}$$

The crosswind-integrated ground level concentration is given by

$$\overline{C}^{y} \sim \frac{Q}{\sigma_z U}. \tag{3.83}$$

The crosswind-integrated concentration is relevant to long line sources of pollution such as roads. Using Eq. (3.80), we obtain the relationship

$$\overline{C}^{y} \sim \frac{Q}{u_* x}. \tag{3.84}$$

This result, which has been derived using other methods by Van Ulden (1978) and Briggs (1982), implies that the concentration of an inert pollutant emitted from a line source, such as a road, falls off linearly with distance from the source. This does not mean that the vertical spread of a plume increases linearly with distance as we see from Eq. (3.85):

$$\sigma_z \sim \frac{u_* x}{U}. \tag{3.85}$$

This equation is implicit in $\sigma_z$ because the wind speed, $U$, on the right-hand side of the equation is also a function of $\sigma_z$ in addition to the roughness length, $z_0$. Because $U$ increases with $\sigma_z$, we expect $\sigma_z$ to grow less than linearly with distance.

In anticipation of the other expressions derived in this chapter, we rewrite Eq. (3.83) using the following definitions:

$$\overline{C_*}^{y} = \frac{\overline{C}^{y} u_* |L|}{Q}, x_* = x/|L|, \tag{3.86}$$

where $L$ is the Monin−Obukhov length. Then the behavior of the ground-level concentrations under neutral condition is described by

$$\overline{C_*}^{y} \sim x_*^{-1}. \tag{3.87}$$

## The Unstable Surface Boundary Layer

To extend our previous analysis to other stabilities we will use the following approach. We will first derive the equations for $\sigma_z$ assuming the surface layer is very unstable or very stable (small $|L|$). Then, we will interpolate between the neutral and the asymptotically stable or unstable expressions to obtain a formula for the entire range of stabilities. Let us illustrate the application of this approach to derive expressions for

$\sigma_z$ and the crosswind-integrated concentration for a release in the unstable surface layer.

Under asymptotically unstable conditions, the eddy diffusivity of heat as a function of height is given by

$$K_H(z) \sim u_* z(-z/L)^{1/2}. \tag{3.88}$$

Then Eq. (3.75) for asymptotically unstable conditions becomes

$$U\frac{d\sigma_z^2}{dx} \sim u_*\sigma_z(-\sigma_z/L)^{1/2} \tag{3.89}$$

or

$$\frac{d\sigma_z}{dx} \sim \left(\frac{u_*}{U}\right)\sigma_z{}^{1/2}|L|^{-1/2}. \tag{3.90}$$

Assuming $\left(\frac{u_*}{U}\right)$ approaches a constant value, integrating Eq. (3.90) yields

$$\sigma_z \sim \left(\frac{u_*}{U}\right)^2 x^2|L|^{-1}. \tag{3.91}$$

We can write the expression for the crosswind-integrated concentration as

$$\overline{C}^y \sim \frac{Q}{\sigma_z U} \sim \frac{Q|L|U}{u_*^2 x^2}, \tag{3.92}$$

which in terms of nondimensional variables becomes

$$\overline{C_*}^y \sim \left(\frac{U}{u_*}\right)x_*^{-2}. \tag{3.93}$$

Then, an analytical form that interpolates between the neutral and very unstable limits and fits observations is

$$\sigma_z = 0.57\frac{u_*}{U}x\left(1 + 2\left(\frac{u_*}{U}\frac{x}{|L|}\right)\right) \text{ for unstable conditions.} \tag{3.94}$$

We next derive the equations for vertical spread in the stable surface boundary layer.

## The Stable Surface Boundary Layer

Under highly stable conditions, $U$ and $K_H$ can be expressed as

$$K_H \sim u_* L \text{ and } U \sim u_* z/L. \tag{3.95}$$

Substituting this expression in Eq. (3.75) for the rate of growth we obtain

$$u_*(\sigma_z/L)\frac{d\sigma_z^2}{dx} \sim u_* L \tag{3.96}$$

or

$$\frac{d\sigma_z^3}{dx} \sim L^2. \tag{3.97}$$

Integrating Eq. (3.97), we obtain

$$\sigma_z^3 \sim xL^2 \tag{3.98a}$$

or

$$\sigma_z \sim x^{1/3}L^{2/3}. \tag{3.98b}$$

Note that $\sigma_z$ grows as $x^{1/3}$ under very stable conditions. Using this relationship for $\sigma_z$, we can write $U\sigma_z$ as

$$U(\sigma_z) \sim u_*\sigma_z/L \sim u_*(x/L)^{1/3}. \tag{3.99}$$

Then,

$$U\sigma_z \sim u_* x^{2/3}L^{1/3}. \tag{3.100}$$

The expression for the crosswind-integrated ground level concentration becomes

$$\overline{C}^y \sim \frac{Q}{\sigma_z U} \sim \frac{Q}{u_* x^{2/3}L^{1/3}} \tag{3.101}$$

and in terms of nondimensional variables, Eq. (3.101) can written as

$$\overline{C_*}^y = x_*^{-2/3}. \tag{3.102}$$

An expression that interpolates between the neutral and the stable asymptotes for $\sigma_z$ and also describes observed data is given by

$$\sigma_z = 0.57\frac{u_*}{U}x\frac{1}{\left(1+3\frac{u_*}{U}\left(\frac{x}{L}\right)^{2/3}\right)} \text{ for stable conditions.} \tag{3.103}$$

We mentioned earlier that the equations for plume spread are implicit in $\sigma_z$ because the wind speed, $U$, is evaluated at a height proportional to $\sigma_z$.

The preceding equations apply primarily to near surface releases because we have assumed that $\overline{z} \sim \sigma_z$. We can extend these equations to finite height releases by evaluating the wind speed, $U$, at a fraction of the mean plume height, $\overline{z}$, which for a Gaussian vertical distribution of concentrations is related to $\sigma_z$ through the implicit equation

$$\frac{\overline{z}}{\sigma_z} = \sqrt{\frac{2}{\pi}} exp\left[-\frac{1}{2}\left(\frac{h_e}{\sigma_z}\right)^2\right] + \frac{h_e}{\sigma_z} erf\left(\frac{h_e}{\sqrt{2}\sigma_z}\right), \tag{3.104}$$

where $h_e$ is the effective source height.

We now derive expressions for horizontal spread in the surface boundary layer using some of the techniques used for vertical spread.

## Horizontal Spread in the Surface Boundary Layer

The formulation of the horizontal spread equations is based on the results obtained by Eckman (1994) who showed that the variation of $\sigma_y$ with distance and the initial linear increase followed by a smaller increase with distance (or travel time) could be explained by the increase of the wind speed with height if one assumed that $\sigma_y$ is governed by the expression

$$\frac{d\sigma_y}{dx} = \frac{\sigma_v}{U}, \tag{3.105}$$

where $\sigma_v$ is the standard deviation of the horizontal velocity fluctuations, and the transport wind speed, $U$, is evaluated at a fraction of $\sigma_z$.

Under neutral conditions, we can rewrite Eq. (3.105) as

$$\frac{d\sigma_y}{dx} = \frac{\sigma_v}{u_*}\left(\frac{u_*}{U}\right) \sim \frac{\sigma_v}{u_*}\frac{d\sigma_z}{dx} \tag{3.106}$$

resulting in

$$\sigma_y \sim \frac{\sigma_v}{u_*}\sigma_z. \tag{3.107}$$

The asymptotic expression for unstable conditions follows from

$$\frac{d\sigma_y}{dx} = \frac{\sigma_v}{u_*}\left(\frac{u_*}{U}\right). \tag{3.108}$$

As before, assuming that $u_*/U$ is independent of $x$, we can integrate Eq. (3.108) to obtain

$$\sigma_y \sim \frac{\sigma_v}{u_*}\left(\frac{u_*}{U}x\right). \tag{3.109}$$

The bracketed term in Eq. (3.109) can be rewritten using Eq. (3.91) for $\sigma_z$ to obtain

$$\sigma_y \sim \frac{\sigma_v}{u_*}(\sigma_z|L|)^{1/2}. \tag{3.110}$$

The formulation of the stable asymptote for $\sigma_y$ uses

$$\frac{u_*}{U} \sim \frac{L}{\sigma_z} \text{ and } \sigma_z \sim L^{2/3}x^{1/3} \tag{3.111}$$

in Eq. (3.103) to obtain

$$\sigma_y \sim \frac{\sigma_v}{u_*}\frac{\sigma_z^2}{L}. \tag{3.112}$$

We can combine the preceding equations to obtain formulations for $\sigma_y$ for the entire range of $L$. Then, the plume spread equations with the empirical constants that provide the best fit between model estimates and observations become, for stable conditions,

$$\sigma_y = 1.6\frac{\sigma_v}{u_*}\sigma_z\left(1 + 2.5\frac{\sigma_z}{L}\right), L > 0. \tag{3.113}$$

The formulation for $\sigma_y$ for stable conditions that interpolates between neutral and unstable conditions is

$$\sigma_y = 1.6\frac{\sigma_v}{u_*}\sigma_z\left(1 + \frac{\sigma_z}{|L|}\right)^{-1/2}, \; L < 0. \tag{3.114}$$

The preceding equations describe plume spreads measured in field studies in which tracers were released over uniform flat terrain. Thus, the question arises as to whether these equations apply to nonuniform urban conditions. It is likely that the plume spreads in urban areas will deviate from the results of these equations, but in the absence of a theory for nonuniform urban conditions, the best we can do is to use these equations with the meteorological inputs corresponding to the area being considered. However, these equations cannot be applied in the presence of building structures, such as street canyons, that induce three-dimensional flows.

## CONCLUDING REMARKS

Air quality models used in practice for source–receptor distances of a few kilometers assume that emissions from a source can be described by a plume in which the concentration distributions in the horizontal and vertical follow the Gaussian distribution; as we have seen, other distributions can be used to describe the vertical concentration profile. This framework allows the incorporation of several processes that affect ground-level concentrations. It can be readily used to interpret data from field studies and thus can be improved empirically to provide better descriptions of dispersion. These features, coupled with its computational simplicity, explain its popularity in applications that require realism as well as transparency.

Highways and roads situated in urban areas are usually lined by sound barriers and can be depressed or elevated relative to the surroundings. These configurations have major effects on dispersion of emissions from the road and hence on near-road air quality. Chapter 4, The Impact of Highways on Urban Air Quality, deals with these effects.

## REFERENCES

Barad M.L. (Ed.), 1958. Project Prairie Grass. A field program in diffusion, Geophysical Research Paper No. 59, vols. I (300 pp.) and II (221 pp.), AFCRF-TR-58-235, Air Force Cambridge Research Center, Bedford, MA.

Briggs, G.A., 1982. Similarity forms for ground-source surface-layer diffusion. Bound. Layer Meteorol. 23, 489–502.

Businger, J.A., 1973. In: Haugen, D.A. (Ed.), Turbulent transfer in the atmospheric surface layer, workshop on micrometeorology. American Meteorological Society, pp. 67–100.

Businger, J.A., Wyngaard, J.C., Izumi, Y., Bradley, E.F., 1971. Flux-profile relationships in atmospheric surface layer. J. Atmos. Sci. 28, 181–189.

Cimorelli, J.A., Perry, G.S., Venkatram, A., Weil, C.J., Paine, J.R., Wilson, B.R., et al., 2005. AERMOD: a dispersion model for industrial source applications. Part I: General model formulation and boundary layer characterization. J. Appl. Meteorol. 44, 682–693.

Eckman, R.M., 1994. Re-examination of empirically derived formulas for horizontal diffusion from surface sources. Atmos. Environ. 28, 265–272.

Gryning, S.E., Van Ulden, A.P., Larsen, S., 1983. In: Model, A.K. (Ed.), Dispersion from a ground level source investigated, vol. 109. Quart. J. R. Meteorol. Soc., pp. 355–364.

McElroy, J.L., Pooler, F., 1968. The St. Louis dispersion study-volume II—analysis. National Air Pollution Control Administration, Pub. No. AP-53, US DHEW Arlington, 50 pps.

Nieuwstadt, F.T.M., 1981. The steady state height and resistance laws of the nocturnal boundary layer: theory compared with Cabauw observations. Bound. Layer Meteorol. 20, 3–17.

Nieuwstadt, F.T.M., 1984. The turbulent structure of the stable, nocturnal boundary layer. J. Atmos. Sci. 41, 2202–2216.

Nieuwstadt, F.T.M., Van Ulden, A.P., 1978. A numerical study of the vertical dispersion of passive contaminants from a continuous source in the atmospheric surface layer. Atmos. Environ. 12, 2119–2124.
Panofsky, H.A., Tennekes, H., Lenschow, D.H., Wyngaard, J.C., 1977. The characteristics of turbulent velocity components in the surface layer under convective conditions. Bound. Layer Meteorol. 11, 355–361.
Pasquill, F., 1961. The estimation of the dispersion of windborne material. Meteor. Mag. 90, 33–49.
Stull, R., 1988. An Introduction to Boundary Layer Meteorology. Springer, The Netherlands.
Van Ulden, A.P., 1978. Simple estimates for vertical dispersion from sources near the ground. Atmos. Environ. 12, 2125–2129.
Van Ulden, A.P., Holtslag, A.A.M., 1985. Estimation of atmo- spheric boundary-layer parameters for diffusion applications. J. Clim. Appl. Meteorol. 24, 1196–1207.

## FURTHER READING

Calder, L.K., 1973. On estimating air pollution concentrations from an highway in an oblique wind. Atmos. Environ. 7, 863–868.
Csanady, G.T., 1973. Turbulent Diffusion in the Environment. Reidel, Dordrecht, p. 248.
Esplin, J.G., 1995. Approximate explicit solution to the general line source problem. Atmos. Environ. 29, 1459–1463.
Holtslag, A.A.M., Van Ulden, A.P., 1983. A simple scheme for daytime estimates of the surface fluxes from routine weather data. J. Climate Appl. Meteorol. 22, 517–529.
Luhar, K.A., Patil, R.S., 1989. A general finite line source model for vehicular pollution prediction. Atmos. Environ. 23, 555–562.
Perry, S.G., 1992. CTDMPLUS: a dispersion model for sources in complex topography. Part I: Technical formulations. J. Appl. Meteor. 31, 633–645.
Schulman, L.L., Strimaitis, D.G., Scire, J.S., 2000. Development and evaluation of the PRIME Plume Rise and building downwash model. JAPCA J Air Waste Manag. Assoc. 50, 378–390.
Snyder, W.H., Thompson, R.S., Eskridge, R.E., Lawson, R.E., Castro, I.P., Lee, J.T., et al., 1985. The structure of the strongly stratified flow over hills: dividing streamline concept. J. Fluid Mech. 152, 249–288.
Taylor, G.I., 1921. Diffusion by continuous movements. Proc. London Math. Soc., Ser. 2 (20), 196–211.
Venkatram, A., 1980. Estimating the Monin–Obukhov length in the stable boundary layer for dispersion applications. Boundary-Layer Meteorol. 19, 481–485.
Venkatram, A., 1992. Vertical dispersion of ground-level releases in the surface boundary layer. Atmos. Environ. 26, 947–949.
Venkatram, A., 1993. Estimates of the maximum ground level concentration in the convective boundary layer—the error in using the Gaussian distribution. Atmos. Environ. 27A, 2187–2191.
Venkatram, A., Horst, T.W., 2006. Approximating dispersion from a finite line source. Atmos. Environ. 40, 2401–2408.
Venkatram, A., Brode, R., Cimorelli, A., Lee, R., Paine, R., Perry, S., et al., 2001. A complex terrain dispersion model for regulatory applications. Atmos. Environ. 35, 4211–4221.
Weil, J.C., 1985. Updating applied diffusion models. J. Climate Appl. Meteor. 24 (11), 1111–1130.
Weil, J.C., 1988. In: Venkatram, A., Wyngaard, J.C. (Eds.), Plume Rise. Lectures on Air Pollution Modeling. American Meteorological Society, Boston, MA, pp. 119–166.